J. Chem. Chem. Eng. 8 (2014) 1068-1081
doi: 10.17265/1934-7375/2014.11.007

Synthesis and Characterization of Trithiocarbonate-Organoclays Nanohybrids and Their Interaction with MCF-7 Cancer Cells

Ulviye Bunyatova[1], Zakir Rzayev[2*], Mustafa Türk[3] and Abdullah Ernur Söylemez[2]

1. Department of Biomedical Engineering, Faculty of Engineering, Baglica Campus, Baskent University, Ankara 06810, Turkey

2. Institute of Science & Engineering, Division of Nanotechnology and Nanomedicine, Beytepe Campus, Hacettepe University, Ankara 06800, Turkey

3. Department of Biology, Division of Bioengineering, Faculty of Science, Kirikkale University, Kirikkale 71450, Turkey

Abstract: This work presents a new approach for the fabrication of organic/inorganic nanohybrids as anticancer drugs by an intercalation method using *S,S*-bis(α,α'-dimethyl-α"-acetic acid) (trithiocarbonate) as a modifier and two organoclays, such as reactive octadecylamine/MMT (montmorillonite) and non-reactive dimethyldidodecyl ammonium/MMT. The chemical and physical structures and the surface morphology of these covalently and non-covalently linked nanohybrids were investigated by FT-IR (Fourier transform infrared) spectroscopy, ^{13}C and ^{29}Si solid state NMR (nuclear magnetic resonance) spectroscopy, XRD (X-ray powder diffraction) and SEM (scanning electron microscopy) analyses, respectively. To evaluate the anticancer activities of the novel BATC/organoclay hybrids against MCF-7 breast cancer cells, a combination of different biochemical and biophysical testing techniques were used. Cell proliferation and cytotoxicity were detected *in vitro* using a real-time analysis. Cell death was confirmed by using apoptotic and necrotic analyses, the effects of which were determined by the double staining and Annexin-V-FLUOS testing method. The results demonstrate that intercalated hybrid complexes containing a combination of various anticancer sites, such as free and complexed carboxyl, trithiocarbonate, amine and ammonium cations significantly induced cell death in breast cancer via their interactions with the DNA macromolecules of cancer cells by destroying the self-assembled structure of growing cells. Fabricated hybrid complexes may represent a new generation of effective and selective anticancer drug systems with a synthetic/natural origin for cancer chemotherapy.

Key words: Synthesis, intercalating, trithiocarbonate, organoclays, nanohybrids, MCF-7 breast cancer cells, real-time cytotoxicity, apoptosis, necrosis.

Graphical Abstract

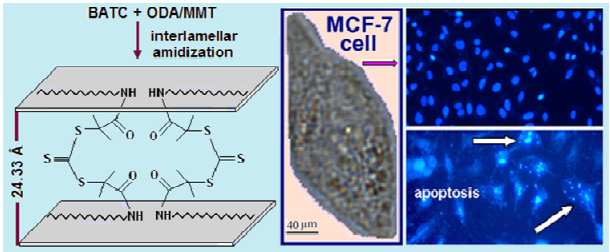

Effect of BATC/ODA-MMT covalence nanohybrid on apoptosis of MCF-7 breast cancer cells.

*Corresponding author: Zakir Rzayev, Professor, research fields: material nanoscience, nanotechnology and nanomedicine. E-mail: rzayevzmo@gmail.com; zmo@hacettepe.edu.tr.

1. Introduction

Many researchers believe that MMT (montmorillonite) mineral clay played an important role in the origin of life, as a catalyst, in synthesis, selecting, protecting and concentrating biomacromolecules under the natural conditions. MMT adsorbing organic compounds also catalyze a variety of organic reactions critical to the origin of life [1-3]. Ferris demonstrated that MMT intercalated with RNA (ribonucleic acid) molecules can catalyze the formation of biomacromolecules with relatively high molecular weights. He also found that MMT with alkali and alkaline earth metal ions, as exchangeable

cations, was catalytically more active than pristine MMT with iron and other transition metal ions as exchangeable cations. According to Ferris's theory, life based on RNA precedes current life, which is based on DNA and proteins [3]. Because of the unique properties of DNA/MMT clay complexes, many researchers have a great interest in the use of these complexes, especially DNA/organo-MMT complexes in gene delivery systems as non-viral vectors [4-7]. Lin et al. [4] synthesized DNA/organo-MMT complexes by the intercalation of hexadecyltrimethyl ammonium into the interlayer of MMT clay. They demonstrated that DNA was successfully transfected into the nucleus of human dermal fibroblasts and enhanced green fluorescent protein expression, leading to green fluorescence emission. According to the authors, the modified MMT clay has great potential for gene delivery in the future. Presently, there is a considerable number of scientific publications on the unique properties of clay minerals, especially MMT clay and its organic derivatives as well as their utilization in pharmaceutical formulations and cosmetics [8-11] in medicine as carriers for antibacterial [12-15] and anticancer agents [16, 17]; in drug and gene delivery systems as targeting agents [18-20]; and in tissue engineering for drug targeting [21]. Modified MMT inhibits intestinal absorption of cholesterol on the nano-scale [22] and absorbs uric acid [23]. According to Feng et al. [24, 25], one of the most common side effects of cancer chemotherapy is gastrointestinal problems, which lead to microsites and ulceration of the gastrointestinal tract and diarrhea. They developed a novel bioadhesive drug delivery system, poly (D, L-lactide-co-glycolide)/MMT nanoparticles, for the oral delivery of paclitaxel. These nanoparticles were prepared by the emulsion/solvent evaporation method. The authors also developed four systems of biodegradable polymers for the oral delivery of anticancer drugs, which include poly (lactic-*co*-glycolic acid) (NP-I), poly (lactic)-PEG modified vitamin E (NP-II), poly (lactic-*co*-glycolic acid)-MMT (NP-III) and poly (lactic)-PEG modified vitamin E-montmorillonite (NP-IV) nanoparticles. Lin et al. [26] observed that MMT was non-toxic by hematological, biochemical and histopathological analyses in rat models. Lee et al. [27, 28] reported that MMT-$^{+}$Na could be used as a drug carrier for controlled release systems, and they investigated yeast and rats model for pharmaceutical applications.

Many known biomolecular cytotoxic anticancer drugs exhibit severe side effects due to their non-selective interaction with tumor cells. To improve the selectivity of drugs and anticancer agents in bioengineering processing, many researchers have used (bio)organically modified MMT clays, such as MMT intercalated with hexadecyltrimethyl ammonium [5], plasmid DNA [6, 7], vitamin-E1 [27] and 5-fluoroacil [28]. On the other hand, some cationic amphiphilic surfactants, such as DDAB (didodecyldimethyl ammonium bromide) [29-31], are potent inducers of cell death and apoptosis in a wide range of tumor cell lines. DDAB, as a surfactant, has also been widely used in the fabrication of polymer layered silicate nanocomposites [32, 33]. Recently, researchers have developed new biocompatible nanoparticle drug carriers with efficiently encapsulated antitumor drug molecules and have been able to control their release at the specific site of action [34-38].

The synthesis, characterization and anticancer activity of functional copolymers with organoboron, carboxyl/anhydride, pyran, dioxalane, smart *N*-isopropyl acrylamide and end trithiocarbonate functionalities were the subjects of our recent systematic publications [39-41]. We have demonstrated that end trithocarbonate and carboxyl functionalized and partially decarboxylated poly (maleic anhydride) exhibits highly selective anticancer activity (cytotoxicity, apoptotic and necrotic effects) towards HeLa cells and almost non-toxicity for normal cells (fibroblast cells) [41].

A goal of this work was the synthesis and

characterization of novel intercalated complexes of ODA-MMT (octadecyl amine-MMT) and DMDA-MMT (dimethyl didodecyl ammonium bromide-MMT) with BATC...(*S,S*-bis(α,α'-dimethyl-α"-acetic acid) trithiocarbonate) and the evaluation of their cytotoxic, apoptotic and necrotic effects on human breast cancer cells (MCF-7) by using a combination of physical and biochemical analysis methods. Another aspect of this work was a comparative analysis of the anticancer activity of pristine organoclays and their intercalated hybrids with BATC.

2. Experiments

2.1 Materials

S,S-bis(α,α'-dimethyl-α"-acetic acid) trithiocarbonate, which is also known as a RAFT (reversible addition-fragmentation fragmentation chain-transfer) agent, was synthesized by a known method [42]. ODA/MMT (octadecyl amine-MMT) clay (Nanomer 1.30 E) and DMDA/MMT (dimethyldidodecyl ammonium/MMT) clay (Nanomer 1.44 P) were purchased from Sigma-Aldrich (Germany) and dried under vacuum at 80 ^{o}C before used. The average characteristics of the ODA/MMT: content of octadecyl amine 25%-30%, bulk density 0.41 g/cm^3, CEC (cation exchange capacity) 95 mEq and crystallinity, 52.8% (by XRD (X-ray powder diffraction)); DMDA/MMT: specific surface area, 43.6 $m^2 \cdot g^{-1}$; specific mesopore volume, 0.14 $m^3 \cdot g^{-1}$; contents of N, 1.12%, and C, 32.56%; and crystallinity, 58.2% (by XRD). All other solvents and reagents were of analytical grade and were used without purification.

MCF-7 cancer cells were obtained from the Division of Bioengineering, Istanbul University, Turkey. Cell culture flasks and other plastic material were purchased from Corning (NY, USA). DMEM (Dulbecco Modified Eagle's Medium) with L-glutamine, FCS (fetal calf serum), Trypsin-EDTA, Hoechst 33342 and PI (propidium iodide) were purchased from Serva (Israel); WST-1 [2-(4-Iodophenyl)-3-(4-nitrophenyl)-5-(2,4-disulfo-phenyl)-2H-tetrazolium] reagent and Annexin-V-FLUOS were purchased from Roche (Germany).

2.2 Synthesis Procedure

S,S-bis(α,α'-dimethyl-α"-acetic acid) trithiocarbonate was synthesized from carbon disulfide, chloroform, acetone, and tricapryl ammonium hydrogen chloride according to a known procedure [42]. Recently, Moad et al. [43] reported the design and synthetic pathways of carboxyl and trithiocarbonate containing compounds as RAFT agents and their macromolecular derivatives as useful for a given polymerization, end functionalization, conjugation and set of reaction conditions, including the esterification of carboxyl groups, the active ester-amine reaction, and a single unit monomer insertion.

The syntheses of the BATC/organoclay nanohybrids were conducted using the following procedure [44]. In brief, BATC/organoclay mixture with a molar ratio of BATC: intercalant (ODA or DMDA) = 1:2 (as a carboxyl/amine equivalent) was dissolved in deionized water (for ODA/MMT) or dispersed in MEK (methyl ethyl ketone) (for DMDA/MMT) by intensive mixing at 50 ^{o}C for 4 h to prepare the intercalated BATC/organoclay nanohybrids. Then, the reaction mixture was treated with a large amount of methanol at room temperature by intensive mixing up to the full precipitation of the powder product, which was isolated by centrifugation-filtration and dried under vacuum at 40 ^{o}C.

2.3 Characterization

The FT-IR (Fourier transform infrared) spectra were recorded on an FT-IR Nicolet 510 spectrometer by the standard KBr disk method over the range of 500-4,000 cm^{-1} with a resolution of 4 cm^{-1}. Solid state ^{13}C NMR spectroscopy with CP (cross-polarization) and MAS (magnetic angle spinning) and ^{29}Si MAS

NMR spectroscopy were performed at 8,500 Hz spin rate and mass probe of 4 mm to collect direct information on the structural characteristics of intercalated BATC/organoclay nanohybrids.

The XRD patterns were performed with a PANanalytical X-ray diffractometer equipped with a CuK_α tube and Ni filter (λ = 1.5406 Å). The XRD patterns were measured at 2θ, in the range 1^o-50^o. The Bragg equation was used to calculate the interlayer spacing (d): $n\lambda = 2d\sin\theta$, where n is the order of reflection and θ is the angle of reflection.

The surface morphology of the nanohybrids was examined using a brief description of the ZEISS SUPRA 40 FESEM (field emission scanning electron microscope) with image scales of 2 μm × 2,000 and 10 μm × 10,000 magnifications using an acceleration voltage of 20 kV. All of the specimens were freeze-dried and coated with a thin layer of platinum before testing by using a QUORUM-Q150R surface coating device.

ODA/MMT clay (Nanomer 1.30 E) and DMDA/MMT clay (Nanomer 1.44 P) were purchased from Sigma-Aldrich (Germany) and dried under vacuum at 80 ^oC before used. The average characteristics of the ODA/MMT: content of octadecyl amine 25%-30%, bulk density 0.41 g/cm^3, CEC 95 mEq and crystallinity, 52.8% (by XRD); DMDA/MMT: specific surface area, 43.6 $m^2 \cdot g^{-1}$; specific mesopore volume, 0.14 $m^3 \cdot g^{-1}$; contents of N, 1.12%, and C, 32.56%; and crystallinity, 58.2% (by XRD). All other solvents and reagents were of analytical grade and were used without purification.

2.4 MCF-7 Cells Cultures

MCF-7 cells were placed in cell culture flasks containing DMEM with L-glutamine, 10% FCS and 1% antibiotic and were kept in a CO_2 incubator conditioned with 5% CO_2 at 37 °C for 48 h. For harvesting the cells, the cell culture medium was discharged, and the cells were treated with trypsin-EDTA (0.5 mL per flask). The cells were then transferred into 15 mL Eppendorf tubes and centrifuged at 1,000 rpm for 3 min. The supernatant was discharged, and the cells were used in the next studies.

2.5 Cell Proliferation and Cytotoxicity Assay

Cell proliferation and cytotoxicity was determined using a RTCA (real-time analyzer) (Roche, Germany) to monitor the cellular responses after treatment with the anti-cancer agents *in vitro*. MCF-7 cells (10×10^3 cells per well) were cultivated in DMEM-F12 without L-glutamine using an E-Plate 96 (Roche) for cell growth monitoring. The plates were kept in a CO_2 incubator (37 °C in 5% CO_2) during the experiment. After 19 h of incubation, different amounts of ODA/MMT and DMDA/MMT and their intercalated hybrids BATC...ODA/MMT and BATC...DMDA/MMT (approximately 0-80 $\mu g \cdot mL^{-1}$ in the medium) were added to the wells containing cells and cultivated at the same conditions. The attachment and logarithmic growth of the cells was monitored every 10 min over 42 h. Half inhibition concentration (IC_{50}) values of the copolymers were determined by the (RTCA)-SP instrument.

2.6 Analysis of Apoptotic and Necrotic Cells

Apoptotic and necrotic analyses were performed by double staining and the Annexin-V-FLUOS testing method. Double staining was performed to quantify the number of apoptotic cells in the culture based on scoring apoptotic cell nuclei. MCF-7 cells (20×10^3 cells per well) were grown in DMEM-F12 with L-glutamine supplemented with 10% fetal bovine serum and 1% penicillin-streptomycin at 37 °C in a 5% CO_2 humidified atmosphere using 48-well plates. MCF-7 cells were treated with different amounts (0, 10, 20, 40 and 80 $\mu g \cdot mL^{-1}$) of ODA-MMT agent and the same amount of BATC…ODA/MMT, DMDA/MMT and BATC…DMDA/MMT for 24 h. Additionally, cancer cells were treated with only cell medium as a control. Both attached and detached cells

were collected and then washed with PBS (phosphate buffer solution) and stained with Hoechst dye 33342 (2 μg·mL^{-1}), propodium iodide (1 μg·mL^{-1}) and free-RNAse DNAse (100 μg·mL^{-1}) for 15 min at room temperature. Then, 10-50 μL of the cell suspension was smeared on a slide and cover slip for examination using fluorescence microscopy. The number of apoptotic and necrotic cells was determined with a fluorescence inverted microscope DMI6000 (Leica) with a DAPI filter and an FITC filter.

2.7 Annexin-V-FLUOS Immunostaining

Annexin-V-FLUOS, a calcium-dependent phosphor- lipid-binding protein with a high affinity for phosphatidyl serine, was used to detect apoptosis. Briefly, MCF-7 cells (10×10^3/well) were seeded into a 48-well plate with DMEM, including 10% FCS. The next day, the medium was discharged and replaced with fresh medium containing 10% FCS, organoclay and their intercalated hybrids ranging from 10 μg·mL^{-1} to 80 μg·mL^{-1}. In the control group, MCF-7 cells were treated with cell culture medium only. After 24 h of treatment, the cell culture medium containing floating cells was collected and centrifuged at 3,000 rpm. Adherent cells were stained in the well. The cells were then washed in PBS and resuspended in binding buffer (10 mm HEPES/NaOH, pH 7.4, 140 mm NaCl, 2.5 mm $CaCl_2$). Annexin-V-fluos and propodium iodide were added to a final concentration of 10 μg·mL^{-1} and 1 μg·mL^{-1}, respectively, and the cells were incubated in the dark for 10 min. The cells were washed again in PBS and resuspended in binding buffer. The numbers of Annexin-V-fluos labeled cells were counted using the 40× objective of an inverted fluorescence microscope (Leica DMI6000, Germany). For each image, three randomly selected microscopic fields were evaluated.

3. Results and Discussion

3.1 Intercalation of BATC between Silicate Layers

The synthetic pathway of intercalated BATC/organoclay nanohybrids can be schematically represented as follows (Fig. 1): the intercalation of BATC molecules between silicate galleries is accompanied with strong complex-formation of ammonium cations from organoclays and free carboxyl groups of BATC. Unlike DMDA/MMT clay, which tends to form strong complexes with BATC, ODA/MMT clay forms hydrogen bonding complexes, which are easily transformed to an amide form by annealing the powder complex after isolation from the reaction mixture.

3.2 Chemical and Physical Structures

The chemical structure of intercalated complexes was confirmed by FTIR spectroscopy. The FTIR spectra of the synthesized complexes are illustrated in Fig. 2.

Agreeing with spectral analysis, the structure of the synthesized intercalated molecular complex of BATC ODA-MMT was confirmed by the following changes of the characteristic bands: (1) new characteristic bands at 2,649 and 2,542 cm^{-1} (stretching of -COOH in the complex); 1,703 cm^{-1} (broad acid C=O stretching in -COO-); 1,619 cm^{-1} (shifting to a high region of NH_2 deformation); 1,507 and 1,408 cm^{-1} (combination of $-H_3N^+$ torsion and $-H_3N^+$antisymmetric deformation), which can be related to complexed $-COO^-\cdot{}^+NH_3-$ linkages; (2) the absorption bands at 3,247 and 3,180 cm^{-1} (NH_2 stretching bands), 2,926 and 2,853 cm^{-1} (CH_2 stretching), and 1,468 (CH_2 deformation); (3) the observed bands at 1,445 cm^{-1} (OH bending), 1,378 and 1,366 cm^{-1} (CH_3 deformation in $-C(CH_3)_2-$), and 1,287 cm^{-1} (C=S stretching in S-(C=S)-S group), which are related to the BATC fragment of the complex; and (4) the characteristic bands at 3,634 cm^{-1} (Si-OH or OH from water molecules). The formation of a new characteristic amide-II band at 1,655 cm^{-1} and the significant decrease of the intensity of the broad carboxylic bands at 1,700 cm^{-1} and 1,507 cm^{-1} are associated with the stretching of the -COO- groups from intercalated BATC…ODA-MMT complex.

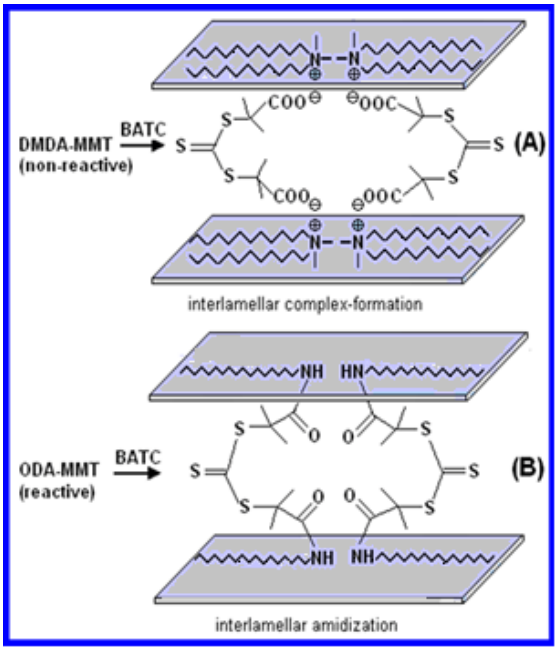

Fig. 1 Synthetic pathway and structure of intercalated BATC/organoclay nanohybrids.

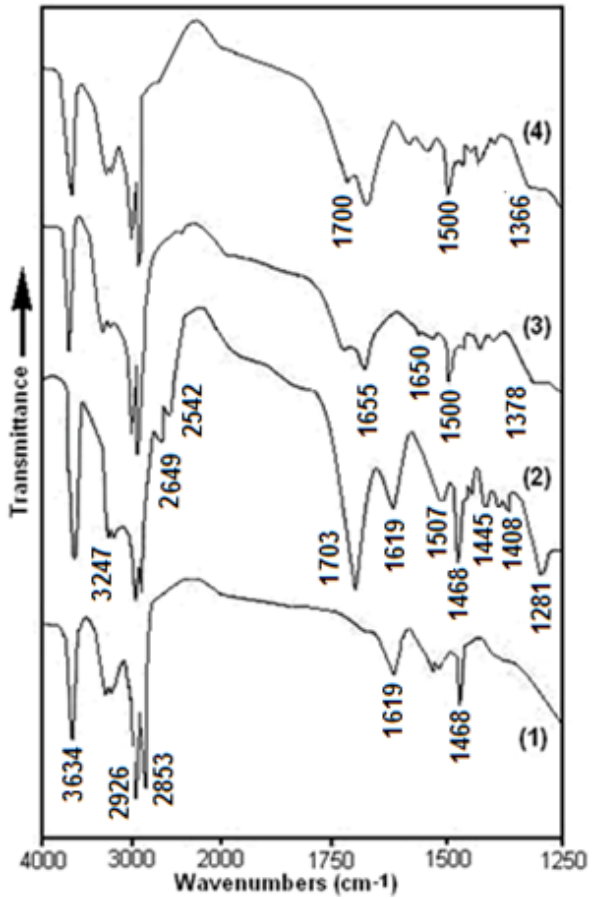

Fig. 2 FTIR spectra of (1) pristine ODA/MMT and BATC…ODA/MMT; (2-4) after annealing at 120 °C for 1 h and 2 h, respectively.

The disappearance of the 2,649 and 2,542 cm^{-1} bands relating to the carboxylic groups in the -NH^{3+}·-OOC- complexes after annealing at 120 °C for 1 and 2 h indicate a complete amidization reaction.

Chemical structure of intercalated BATC…ODA-MMT complex was also confirmed by solid state ^{13}C CPMAS and ^{29}Si NMR MAS spectroscopy (Fig. 3). The isotropic chemical shift of a carbon atom in the hydrogen bonding -COOH·NH_2-·(-COO^-) was observed at 103 ppm; double weak chemical shifts at around 290 ppm can be attributed to the C=O carbon atoms from two carboxyl groups; strong triplet carbon chemical shifts of -COOH were also appear at 175.5 ppm; strong doublet and triplet chemical shifts around 15-18 ppm and at 10.2 ppm associated with four carbon atoms of CH_3 groups and end CH_3 of octadecyl group, respectively; the peaks at 215.9 and 52.3 ppm can be related to the carbon chemical shifts from C=S and $(CH_3)_2$-C- groups, respectively in thrithiocarbonate fragment; -$(CH_2)^{n-}$ carbons from octadecyl group appear around 20-28 ppm. ^{29}Si NMR spectrum of intercalated BATC…ODA/MMT hybrid was simulated with one Gaussian peak with -107 ppm isotropic chemical shift, corresponding to the SiO_2 crystals from MMT clay.

The physical structure of these complexes was determined by the XRD method, and the obtained patterns and diffraction parameters are summarized in Fig. 4.

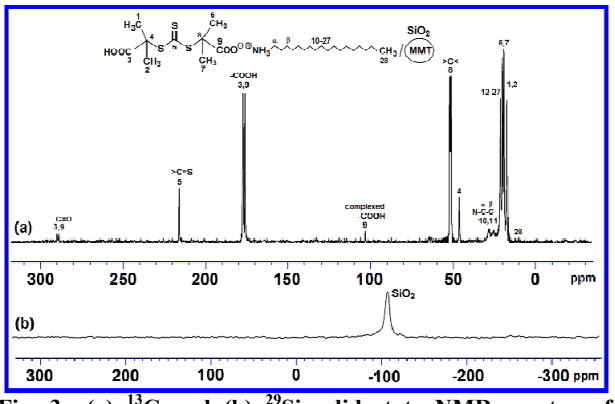

Fig. 3 (a) ^{13}C and (b) ^{29}Si solid state NMR spectra of intercalated BATC…ODA/MMT nanohybrid.

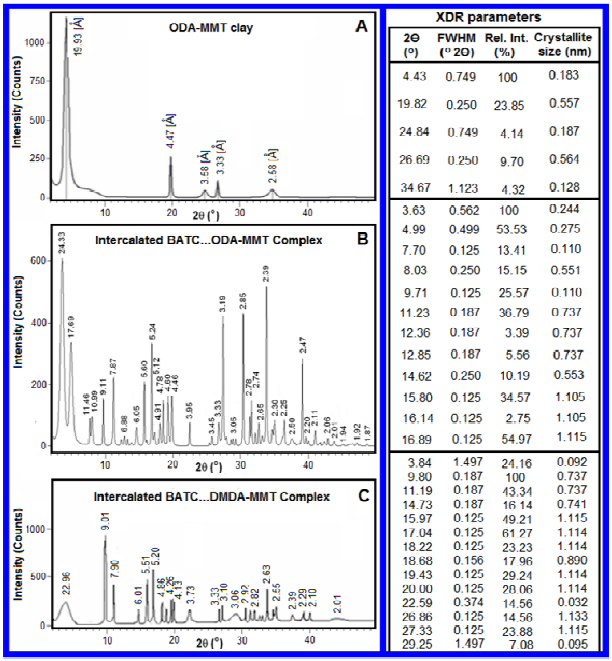

XDR parameters

2Θ (°)	FWHM (° 2Θ)	Rel. Int. (%)	Crystallite size (nm)
4.43	0.749	100	0.183
19.82	0.250	23.85	0.557
24.84	0.749	4.14	0.187
26.69	0.250	9.70	0.564
34.67	1.123	4.32	0.128
3.63	0.562	100	0.244
4.99	0.499	53.53	0.275
7.70	0.125	13.41	0.110
8.03	0.250	15.15	0.551
9.71	0.125	25.57	0.110
11.23	0.187	36.79	0.737
12.36	0.187	3.39	0.737
12.85	0.187	5.56	0.737
14.62	0.250	10.19	0.553
15.80	0.125	34.57	1.105
16.14	0.125	2.75	1.105
16.89	0.125	54.97	1.115
3.84	1.497	24.16	0.092
9.80	0.187	100	0.737
11.19	0.187	43.34	0.737
14.73	0.187	16.14	0.741
15.97	0.125	49.21	1.115
17.04	0.125	61.27	1.114
18.22	0.125	23.23	1.114
18.68	0.156	17.96	0.890
19.43	0.125	29.24	1.114
20.00	0.125	26.06	1.114
22.59	0.374	14.56	0.032
26.86	0.125	14.56	1.133
27.33	0.125	23.88	1.115
29.25	1.497	7.08	0.095

Fig. 4 XRD patterns and parameters of pristine ODA/MMT (A) and BATC/organoclay intercalated hybrids (B and C).

The well-known Scherrer equation is used to calculate the particle size (τ_{sh}, the mean thickness) [45]: $\tau = K_{sh}\lambda/\beta\cos\theta$, where: τ is the mean size of the ordered (crystalline) domains, which may be smaller or equal to the grain size; K is a Scherrer constant (K_{sh} of 0.89); λ is the X-raywavelength (λ = 1.5406 nm); β is the line broadening at half the maximum intensity (FWHM), after subtracting the instrumental line broadening, in radians. Agreeing with the XRD patterns, pristine ODA/MMT clay (Fig. 5a) exhibits a strong peak at $2\theta = 4.45^{o}$, with a distance between two tetragonal layers (d(002)-spacing) of 19.93 Å and several crystallite peaks related to the intermolecular interactions of octadecyl amine and hydroxyl groups from the clay structure via $H_2N\ldots OH$ hydrogen bonding. The number of crystallite peaks dramatically increased after intercalating BATC molecules between the ODA-MMT and DMDA-MMT clay galleries (Figs. 5b and 5c) as a result of the additional interfacial interactions of the two terminal carboxyl groups and the trithiol fragment of the BATC molecules with alkyl amine or alkyl ammonium cations and hydroxyl groups from the inorganic Si-OH at edges. The *d*-spacing values are increased by the intercalation of BATC molecules from 19.93 Å (ODA/MMT) to 24.33 Å (BATC…ODA/MMT). Recently, Moreno-Fuquen et al. [46] reported that the molecular structure of pristine BATC exhibited intramolecular CH…S hydrogen bonds, and pairs of OH…O hydrogen bonds in the crystal led to the formation of centrosymmetric dimers, which were in turn connected by weak CH…O interactions.

3.3 Surface Morphology

SEM images of the surface morphology of intercalated BATC…ODA/MMT and BATC…DMDA/MMT complexes are illustrated in Figs. 5 and 6.

Comparative analysis of the obtained SEM images indicated that the surface morphology of pristine ODA/MMT organoclay contained relatively large domains with particle sizes of approximately 6-8 μm (Fig. 5, right images at different magnifications), whereas intercalated BATC…ODA/MMT complexes showed better compatibizing homogeneous blends of organic and inorganic phases, with a fine distribution of particles (black points) surrounded with BATC

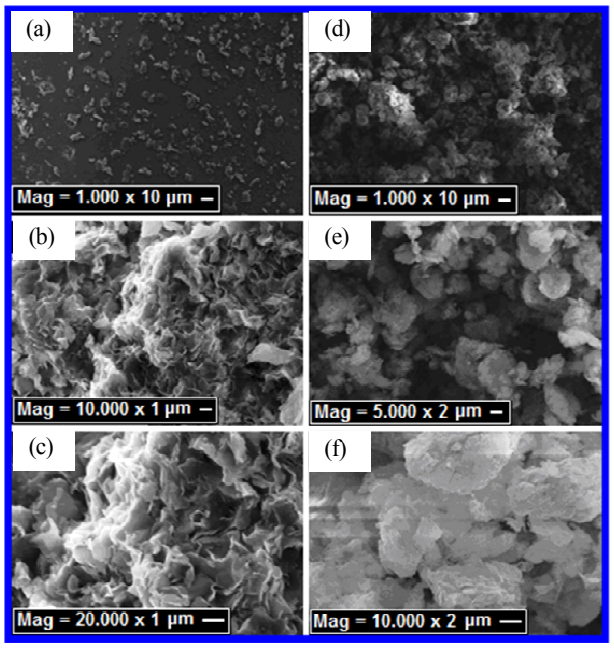

Fig. 5 SEM morphology images of intercalated complex ((a)-(c)) and pristine ODA/MMT ((d)-(f)).

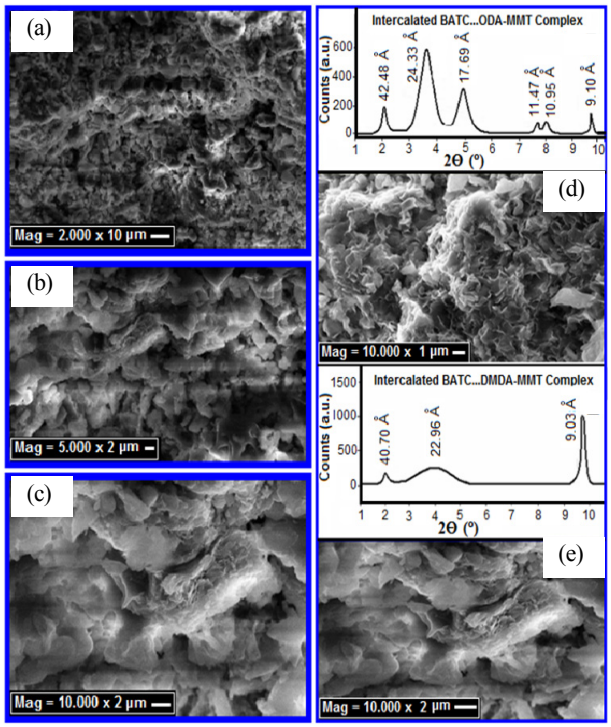

Fig. 6 SEM morphology images ((a), (b) and (c)) and XRD patterns ((d) and (e)) of interclated complexes.

molecules (Fig. 5, left images). These observations can be explained by *in situ* physical (H-bonding) and chemical (amidization) interfacial interactions in the formation of the surface morphology. The SEM morphology images of the BATC…DMDA/MMT complex hybrid indicate the formation of a homogenous blend of organic and inorganic phases but with the formation of large domains (Figs. 6a, 6b, 6c) due to the *in situ* physical interfacial interactions in the generation of the surface morphology. The results of the comparative analysis of XRD (patterns from 1° to 10° 2θ region) and SEM (at higher magnifications), which are illustrated in Figs. 6d and 6e, confirmed the previously mentioned significant difference of the XRD and morphology parameters of the two synthesized nanohybrids. There is suggested that this observed difference in surface morphology and XRD patterns depends on the structural factors, origin of synthesized nanohybrids and the *in situ* processing, which plays an important role in the interactions of nanohybrids with breast cancer cells (MCF-7).

3.4 Evaluation of Cell Proliferation and Cytotoxicity

The cytotoxicity of the organoclays and their intercalated complexes were evaluated in MCF-7 cell lines. According to the RTCA system results, the concentration of the tested samples had a strong impact on cell mortality. The cytotoxicity was determined as the half-maximum inhibiting concentration IC_{50} values from the resulting dose-response curves (Figs. 7a and 7b). Cell index for 42 h for the (c) ODA/MMT and (d) DMDA/MMT organoclays. Cell index monitored every 10 min of 42 h; proliferation plots MCF-7 cells from begining time to 42 h with different concentration of samples (5-80 $\mu g \cdot mL^{-1}$); 20 h later cells were treated with all samples in E-plates (96:1).

Agreeing with the RTCA results, the IC_{50} value of the ODA/MMT and DMDA/MMT organoclays was greater than 80 $\mu g \cdot mL^{-1}$ for MCF-7 cells *in vitro* (Figs. 7c and 7d). The IC_{50} values of the BATC/organoclays were approximately 20 $\mu g \cdot mL^{-1}$ for MCF-7 cells *in vitro* (Figs. 7a and 7b).

The toxicity effect (decrease of the cell index) was observed 2 h after the addition of the BATC…ODA/MMT complex (Fig. 8c) and the BATC…DMDA/MMT complex (Fig. 8d). The BATC BATC…ODA/MMT was more toxic towards MCF-7 cells than the other tested samples. The IC_{50} value of the BATC…DMDA/MMT is 40 $\mu g \cdot mL^{-1}$ for MCF-7 cells. On the other hand, the cell index of the control sample medium-treated MCF-7 (Figs. 7-9) groups (showed in Fig. 9 by the violet curve) increased after another 24 h. Thus, the BATC…ODA/MMT hybrid was more cytotoxic against MCF-7 cells than the organoclays and BATC...DMDA/MMT complex.

Importantly, the BATC…ODA/MMT hybrid exhibited cytotoxicity towards MCF-7 cells *in vitro*. These observations indicate that the designed and synthesized BATC…ODA/MMT exhibits higher cytotoxicity compared with pristine organoclays and the BATC...DMDA/MMT complex at relatively lower concentrations, and it can be described as a potent inducer of MCF-7 cell death.

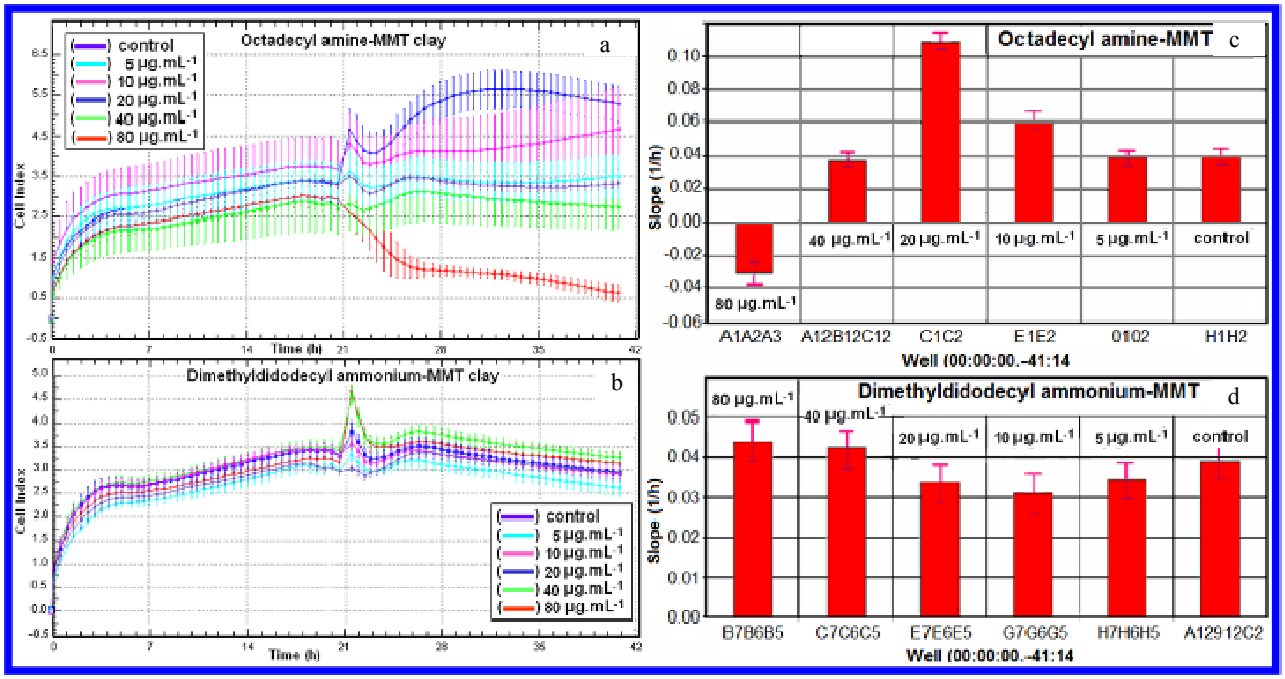

Fig. 7 Dynamic monitoring of MCF-7 cells treated with the organoclays using the RTCA.

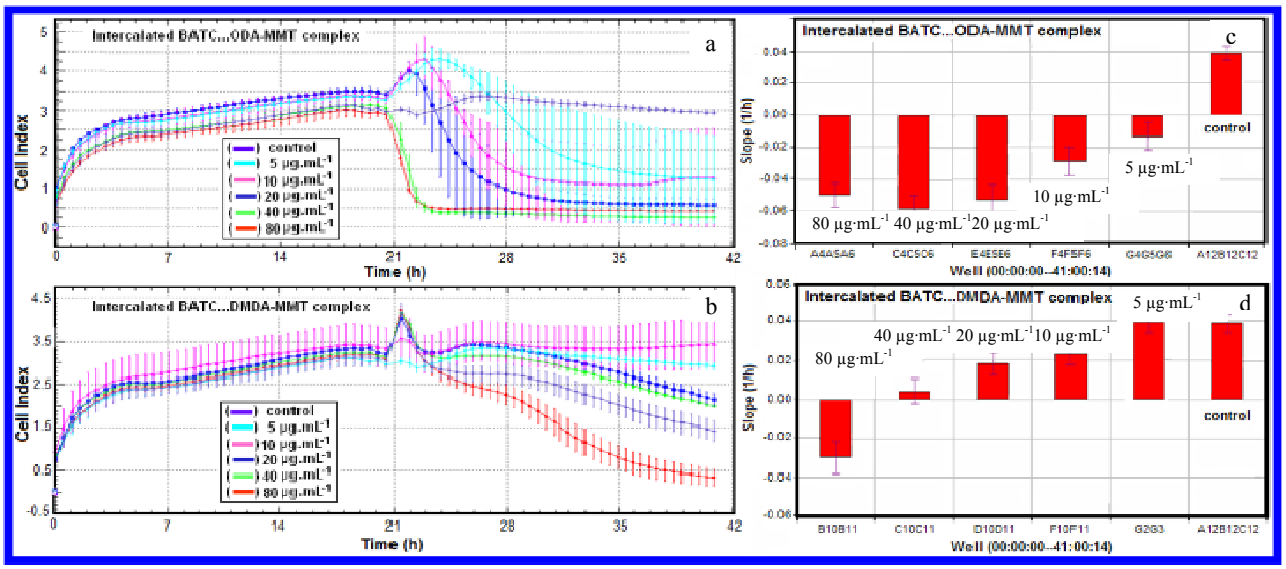

Fig. 8 Dynamic monitoring of MCF-7 cells treated with the BATC/organoclay hybrids using the RTCA.

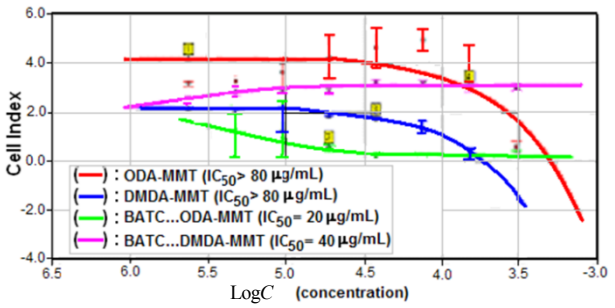

Fig. 9 Cytoxicity (IC_{50}) of the tested organoclays and their intercalated BATC/organoclay hybrids against MCF-7 cells.

3.5 Apoptosis Results

The apoptotic ratio was obtained in two different ways: first, by double staining and second, by Annexin-V-FLUOS staining method. The average values obtained using these methods are summarized in Table 1 (data are expressed as mean ± standard error calculated from three separate experiments), and the fluorescence microscope images are illustrated in

Table 1 Apoptotic and necrotic indexes of (I) ODA/MMT; (II) BATC…ODA/MMT; (III) DMDA/MMT and (IV) BATC...DMDA/MMT with different ratios in MFC-7 cell cultures.

C (μg/ml)	Apoptotic index			
	I	II	III	IV
0	1 ± 1	1 ± 1	1 ± 1	2 ± 1
10	6 ± 1	12 ± 1	5 ± 1	4 ± 1
20	10 ± 2	27 ± 3	9 ± 3	15 ± 2
40	14 ± 1	39 ± 3	2 ± 3	26 ± 2
80	7 ± 1	18 ± 2	9 ± 2	20 ± 2
C (μg/ml)	Necrotic index			
	I	II	III	IV
0	2 ± 2	3 ± 1	1 ± 1	2 ± 1
10	8 ± 2	13 ± 1	4 ± 1	3 ± 1
20	15 ± 2	24 ± 2	7 ± 2	16 ± 1
40	23 ± 2	38 ± 2	13 ± 1	34 ± 2
80	31 ± 4	53 ± 2	17 ± 2	42 ± 2

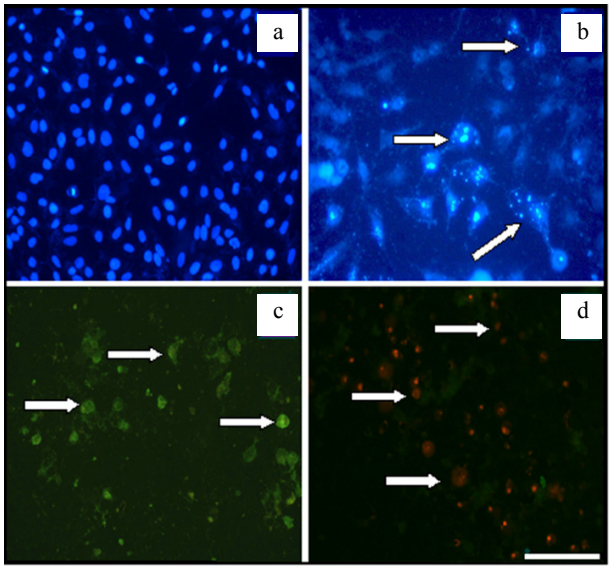

Fig. 10 Apoptotic and necrotic effects of BATC…ODA/MMT hybrid against MCF-7 cancer cells.

Fig. 10. The following testing procedures were used to evaluate the apoptotic and negrotic effects: (a) MCF-7 cells stained with double staining (control group); (b) MCF-7 cells stained with double staining exposed to the BATC…ODA/MMT complex at a concentration of 40 μg·mL^{-1}, where cells undergoing apoptosis are shown by arrows; (c) MCF-7 cells stained by Annexin-V-FLUOS treated with the BATC…ODA/MMT hybrid at a concentration of 40 μg·mL^{-1}, where cells undergoing apoptosis are shown by arrows; (d) MCF-7 cells exposed to the BATC…ODA/MMT hybrid at a concentration of 40 μg·mL^{-1}, where necrosed cell nuclei look red (shown by arrows) stained with PI and non-necrosed cell nuclei look green. Photo-images were taken by Leica DMI6000 inverted fluorescent microscope at 200× magnification.

An apoptotic effect was observed at low concentrations for the intercalated organic clays ODA/MMT and DMDA/MMT and their intercalated hybrids; this effect is increased at higher concentrations. For the BATC…ODA/MMT, the apoptotic effect increased at a concentration up to 40 μg·mL^{-1} (Table 1) but decreased by 3%-18% at higher concentrations (80 μg·mL^{-1}). The latter result can be attributed to the increased cytotoxicity of BATC…ODA/MMT at higher concentrations. Additionally, a stronger apoptotic effect was observed at elevated concentrations of BATC…ODA/MMT compared with high concentrations of the ODA/MMT, DMDA/MMT and BATC...DMDA/MMT samples. Double staining is another method used in determining apoptosis. The Hoechst 33342 fluorescent stain used in this method penetrates the membranes of living cells and stains the nucleus. As a result, nuclei are rendered blue when observed with a DAPI filter under a fluorescent microscope. This technique also enables the evaluation of nuclear morphology. The apoptotic indexes obtained by the double staining and Annexin-V-Fluos methods are summarized in Table 1, and some of the images taken with an inverted fluorescence microscope are collected in Fig. 11. An image from the control group shows no morphological difference in the cell nuclei (Fig. 10a). The apoptotic effect, obtained in parallel with the results of the Annexin-V-Fluos immunocytochemical staining, can be clearly observed, especially for wells where the BATC…ODA/MMT intercalated complex was applied (Fig. 10b). Apoptosis can be clearly distinguished in the images obtained by Annexin-V immunostaining. In particular, Fig. 10c reveals the green color caused by Annexin-V-Fluos staining on

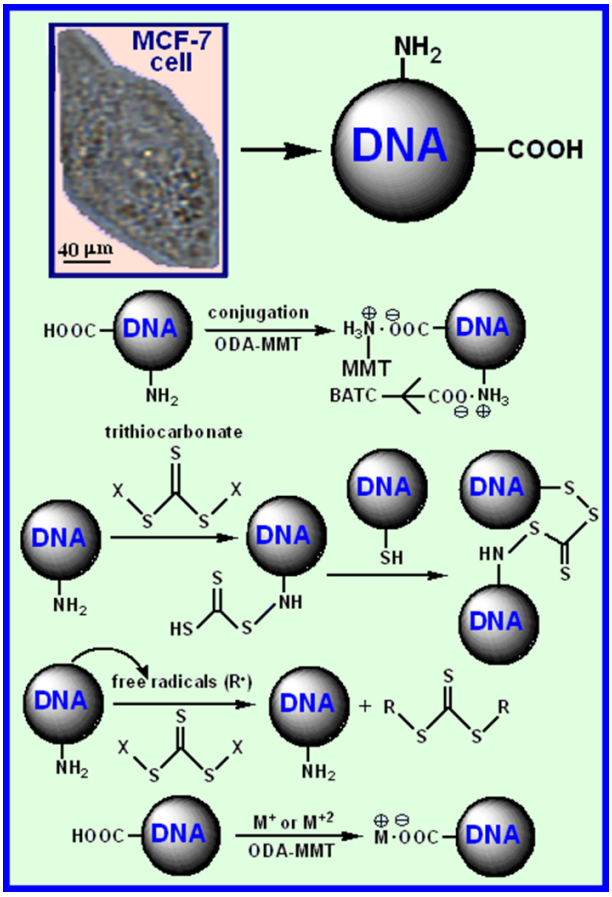

Fig. 11 Chemistry of anticancer active sites and proposed interactions pathways between BATC…ODA/MMT hybrid and MCF-7 cancer cells.

the membrane of apoptotic cells because there was staining by Annexin-V-Fluos antibodies. Thus, in the samples with the BATC…ODA/MMT, the apoptotic cell nuclei decomposed and appeared as a brighter blue color (Fig. 10d) compared to the non-apoptotic cells. The apoptotic effect of the ODA/MMT and DMDA/MMT organoclays and BATC...DMDA/MMT complex (Table 1) was lower compared to that of the BATC…ODA/MMT complex. The highest apoptotic index of approximately 39% ± 3% was obtained for BATC…ODA/MMT at 40 µg·mL^{-1}.

3.6 Necrosis Results

Propodium iodide is an intercalating fluorescent molecule that was used in the double staining and Annexin-V-FLUOS staining methods to detect necrosis in cancer cells subjected to interaction with the ODA/MMT, BATC…ODA/MMT; DMDA/MMT; and the BATC...DMDA/MMT hybrid complex. This stain penetrates dead cells and cells with damaged plasma membranes and causes the nuclei to appear red under fluorescent light. The nuclei of healthy and apoptotic cells appear blue or green when scanned with an FITC fluorescent filter. The necrotic deviation index was examined under fluorescent light (by a FITC filter) at a wavelength of 480-520 nm, where necrotic cell nuclei appeared red and healthy or apoptotic cell nuclei appeared green. The images of necrotic cells are summarized in Fig. 10d, and the necrotic percentage index is provided in Table 1. As observed from these results, the necrotic index is not very high at low concentrations of ODA/MMT and DMDA/MMT organic clays. However, at higher concentrations, a significant increase in toxicity and necrosis was observed. The BATC…ODA/MMT complex had a particularly high necrotic effect. As shown in Table 1, the necrotic effect of the organoclays and the non-covalently incorporated BATC...DMDA/MMT was lower compared with the covalently linked BATC…ODA/MMT nanohybrid. The necrotic effect of nanohybrid was 53% ± 3% at 80 µg·mL^{-1}, whereas a necrotic index of approximately 42% ± 2% was obtained for the obtained for the BATC...DMDA/MMT hybrid complex at 80 µg·mL^{-1}.

3.7 Chemistry of Nanohybrid-Cancer Cell Interactions

The author proposed that the interactions of intercalated complexes with cancer cells can selectively destroy the self-assembly structures of cancer cells and therefore lead to their controlled deaths. The BATC/organoclay hybrids and DNA macro-molecules (MFC-7 cells) include the following important physical and chemical *in situ* reactions: (1) conjugation of the amine and carboxyl groups of complexes with similar groups of cancer cells (DNA macromolecules); (2) reaction of the trithiocarbonate

group with the amine groups of DNA and other active groups and free radicals, which can be formed in cancer cell growth processing; and (3) reaction of ammonium and metal cations at edges of MMT clay with cancer cells. All of these interactions were provided by the relatively high apoptotic and necrotic effects by the use of the covalently incorporated BATC…ODA/MMT nanohybrid compared with the pristine organoclays and the physically incorporated BATC...DMDA/MMT nanohybrid complex, and this nanohybrid can be recommended for future clinical testing as antitumor agents against MCF-7 breast cancer cells.

4. Conclusions

This work presents a facile and effective strategy for the design and synthesis of nanohybrids created by intercalating trithiocarbonate molecules between the silicate galleries of two organoclays: ODA/MMT as a reactive nanofiller and DMDA/MMT as a non-reactive nanofiller. Novel BATC modified organoclay nanohybrids were synthesized. Chemical and physical structures of fabricated hybrid complexes were confirmed. SEM morphology of intercalated nanohybrids strongly depends on the origin of organoclay. Anticancer activity against MCF-7 breast cancer cells of organoclays was evaluated. Comparative analyses show higher activity of BATC…ODA/MMT covalence nanohybrid. FTIR and XRD results indicate that the intercalation of BATC molecules into organoclay has a significant effect on crystallinity of clay and a strong physical and chemical interaction between BATC and ODA/MMT. The intercalated BATC…ODA/MMT easily transformed to the amide form by annealing through amidization of the carboxyl group with octadecylamine intercalant. The nanohybrids exhibit a fine dispersed and homogeneous blended surface morphology due to chemical (predominantly) and physical *in situ* interactions. The synthesized hybrid complexes, containing a combination of anticancer reactive sites, exhibited high cytotoxicity and apoptotic and necrotic effects against human breast MCF-7 cancer cells. The BATC…ODA/MMT complex was more cytotoxic against MCF-7 cells than the organoclays and the BATC...DMDA/MMT complex. Moreover, the BATC…ODA/MMT covalence nanohybrid exhibited cytotoxicity towards MCF-7 cells *in vitro* as a potent inducer of cancer cell death. This nanohybrid also showed the highest apoptotic index and a necrotic effect. Obtained results and proposed chemistry of nanohybrid complex-cancer cell interactions allows us to recommend these carboxyl-trithiocarbonate layered silicate nanohybrids for future clinical testing as effective and selective antitumor agents against MCF-7 breast cancer cells. These topics will be the focus of our future investigations.

Acknowledgments

The authors thank the Turkish Scientific and TUBITAK (Technological Research Council) for the financial support of this work through Projects TBAG-HD/249 and BIDEB-PD/2218.

References

[1] Hazen, R. M. Genesis: Rocks, Minerals, and the Geochemical Origin of Life. *Elements* **2005,** *1*, 135-137.

[2] Hazen, R. M. *Genesis: The Scientific Quest for Life's Origin;* National Academy of Sciences, Joseph Henry Press: Washington, DS, 2005.

[3] Ferris, J. P. Mineral Catalysis and Prebiotic Synthesis: Montmorillonite-Catalyzed Formation of RNA. *Elements* **2005,** *1*, 145-149.

[4] Lin, F. H.; Chen, C. H.; Cheng, W. T. K.; Kuo, T. F. Modified Montmorillonite as Vector for Gene Delivery. *Biomaterials* **2006,** *27*, 3333-3338.

[5] Demameche, S.; Jocteur-Monrozier, L.; Quiquampoix H.; Simonet, P. Evaluation of Biological and Physical Protection against Nuclease Degradation of Clat-Bound Plasmid DNA. *Appl. Environ. Microbiol.* **2001,** *67*, 293-299.

[6] Khanna, M.; G. Stotzky, G. Transformation of Bacillus Subtilis by DNA Bound on Montmorillonite and Effect of Dnase on the Transforming Ability of Bound DNA. *Appl. Environ. Microbiol.* **1992,** *58*, 1930-1939.

[7] Veniale, C.; Lópėz-Galindo, A. Pharmaceutical

Applications of Some Spanish Clays (Sepiolite, Palygorskite, Bentonite): Some Preformulation Studies. *Appl. Clay Sci.* **1999,** *14*, 69-82.

[8] Gámiz, E.; Marcazzan, M.; Linares, J.; Delgado, R. Assessment of Two Spanish Bentonites for Pharmaceutical Uses. *Appl. Clay Sci.* **1992,** *6*, 359-368.

[9] Bettero, A.; Marcazzan, M.; Sementzato, M. Rheologic and Tensiometric Features of Clay Minerals for Thermal and Cosmetic Purposes. Proposal of Protocol for Their Characterization. *Mineralog Petrograph Acta* **1999,** *42*, 277-286.

[10] Veniale, F.; Barberis, E.; Carcangiu, G.; Morandi, N.; Setti, M.; Tessier, D. Formulation of Muds for Pelotherapy Effect of Maturation by Different Mineral Waters. *Appl. Clay Sci.* **2004,** *25,* 135-148.

[11] Cara, S.; Carcangiu, G.; Palomba, M.; Tamanini, M. The Bentonites in Plotherapy Thermal Properties of Clay Pastes from Sardinia (Italy). *Appl. Clay Sci.* **2000,** *16,* 125-132.

[12] Haydel, S. E.; Remenih, C. M.; Williams, L. B. Broad-Spectrum *in Vitro* Antibacterial Activities of Clay Minerals against Antibiotic-Susceptible and Antibiotic-Resistant Bacterial Pathogens. *J. Antimicrob. Chemother.* **2008,** *61,* 353-361.

[13] Yang, He. H.; Yuan, D.; Shen, W. P.; Frost, R. L. A Novel Organoclay with Antibacterial Activity Prepared from Montmorillonite and Chlorhexidini Acetas. *J. Colloid Interface Sci.* **2006,** *297,* 235-243.

[14] Magaa, S. M.; Quintana, P.; Aguilar, D. H.; Toledo, J. A.; Angeles-Chavez, C.; Corts, M. A.; et al. Antibacterial Activity of Montmorillonites Modified with Silver. *J. Molecular Catalysis A: Chemical* **2008,** *281,* 192-199.

[15] Viseras, C.; Aguzzi, C.; Cerezo, P.; Lopez-Galindo, A. Uses of Clay Minerals in Semisolid Health Care and Therapeutic Products. *Appl. Clay Sci.* **2007,** *36,* 37-50.

[16] Forni, F.; Iannuccelli, V.; Coppi, G.; Bernabei, M. T. Effect of Montmorillonite on Drug Release from Polymeric Matrices. *Arch. Parm.* **1989,** *322,* 789-793.

[17] Lee, W. F.; Fu, Y. T. Effect of Montmorillonite on the Swelling Behavior and Drug-Release Behavior of Nanocomposite Hydrogels. *J. Appl. Polym. Sci.* **2003,** *89,* 3652-3660.

[18] Joshi, C. V.; Kevadiya, B. D.; Patel, H. A.; Bajaj, H. A.; Jasra, H. C. Montmorillonite as a Drug Delivery System: Intercalation and *in Vitro* Release of Timolol Maleate. *Int. J. Pharm.* **2009,** *374,* 53-57.

[19] Zheng, J. P.; Wang, C. Z.; Wang, X. X.; Wang, H. Y.; Zhuang, H.; Yao, K. D. Preparation of Biomimetic Three-Dimensional Gelatin/Montmorillonite-Chitosan Scaffold for Tissue Engineering. *React. Func. Polym.* **2007,** *67,* 780-788.

[20] Ducrotte, P.; Dapoigny, M.; Bonaz, B.; Siproudhis, L. Symptomatic Efficacy of Beidellitic Montmorillonite in Irritable Bowel Syndromea Randomized, Controlled Trial. *Aliment Pharm. Ther.* **2005,** *21*, 435-444.

[21] Phillips, T. D.; Lemke, S. L.; Grant, P. G. Characterization of Clay-Based Enterosorbents for the Prevention of Aflatoxicosis. *Adv. Exp. Med. Biol.* **2002,** *504,* 157-171.

[22] Bhattacharyya, K. G.; Gupta, S. S. Adsorption of a Few Heavy Metals on Natural and Modified Kaolinite and Montmorillonite: A Review. *Adv. Colloid Interface Sci.* **2008,** *14,* 114-131.

[23] Yu, D. Y.; Xu, Z. R.; Yang, X. G. *In Vitro*, *in Vivo* Studies of Cu(II)-Exchanged Montmorillonite or the Removal of Lead (Pb). *Animal Feed Sci. Technol.* **2006,** *127,* 327-335.

[24] Dong, Y.; Feng, S. S. Poly(D,L-Lactide-*co*-Glycolide)/Montmorillonite Nanoparticiles for Oral Delivery of Anticancer Drugs. *Biomaterials* **2005,** *26,* 6068-6076.

[25] Feng, S. S.; Mei, L.; Anitha, P.; Gan, C. W.; Zhou, W. Poly(lactic)-Vitamin E Derivative/Montmorillonite Nanoparticles Formulations for the Oral Delivery of Docetaxel. *Biomaterials* **2009,** *30,* 3297-3306.

[26] Lin, F. H.; Lee, Y. H.; Jian, C. H.; Wong, J. M.; Shieh, M. J.; Wang, C. Y. A Study of Purified Montmorillonite Intercalated with 5-Fluorouracil as Drug Carrier. *Biomaterials* **2002,** *23,* 1981-1987.

[27] Lee, Y.; Kuo, T.; Chen, B.; Feng, Y.; Wen, Y.; Lin, W.; et al. Toxicity Assessment of Montmorillonite as a Drug Carrier for Pharmaceutical Applications: Yeast and Rats Model. *Biomed. Eng.-Appl. Basis and Commun.* **2005,** *17,* 12-18.

[28] Lee, Y. H.; Chen, F. H.; Lin, K. Y.; Lin, K. F. Cytotoxic Assessment of L-Ascorbic Acid/Montmorillonite upon Human Dermal Fibroblasts *in Vitro*: MTT Activity Assay. *Biomed. Eng. Appl. Basis and Commun.* **2008,** *20,* 337-343.

[29] Kusumoto, K.; Ishikawa, T. Didodecyldimethyl Ammonium Bromide Induces Caspase-Mediated Apoptosis in Human Leukemia HL-60 Cells. *J. Control Release* **2010,** *147,* 246-252.

[30] Mizuarai, S. K.; Ono, K. J.; You, J.; Kamihira, M.; Iijima, S. Potamine-Modified DDAB Lipid Vesides Promote Gene Transfer in the Presence of Serum. *J. Biochem.* **2001,** *129,* 125-132.

[31] Szala, S.; Missol, E.; Sochanik, A.; Strozyk, M. The Use of Cationic Liposomes DC-CHOL/DOPE and DDAB/DOPE for Direct Transfer of Escherichia Coli Cytosine Deaminase Gene into Growing Melanoma Tumors. *Gene Ther*. **1996,** *3,* 1026-1131.

[32] Rzayev, Z. M. O. Polyolefin Nanocomposites by Reactive Extrusion. In *Advances in Polyolefin*

Nanocomposites; Mittal, V. Ed.; CRC Press, Taylor & Francis Group: New York, 2011; pp 87-127.

[33] Kusmono, Z. A.; MohdIshak, W. S.; Chow, T.; Takeichi, R. Effect of Clay Modification on the Morphological, Mechanical and Thermal Properties of Polyamide/Polypropylene/Montmorillonite Nanocompo-Sites. *Polym. Comp.* **2010,** *31,* 1156-1167.

[34] Farokhzad, O. C.; Langer, R. Impact of Nanotechnology on Drug Delivery. *ACS Nano* **2009,** *3,* 16-20.

[35] Gref, R.; Duchêne, D. Cyclodextrins as "Smart" Components of Polymer Nanoparticles. *J. Drug Delivery Sci. Technol.* **2012,** *22,* 223-233.

[36] Horcajada, P.; Gref, R.; Baati, T.; Allan, P. K.; Maurin, G.; Couvreur, P.; et al. Metal-Organic Frameworke in Medicine. *Chem. Rev.* **2011,** *112,* 1232-1268.

[37] Salvador-Morales, C.; Valencia, P. M.; Thakkar, A. B.; Swanson, E.; Langer, R. Recent Developments in Multifunctional Hybrid Nanoparticles: Opportunities and Challenges in Cancer Therapy. *Front. Biosci.* **2012,** *E4,* 529-545.

[38] Hubbell, J. A.; Chilkoti, A. Nanomaterials for Drug Delivery. *Science* **2012,** *337,* 303-305.

[39] Türk, M.; Rzayev, Z. M. O.; Khalilova, S. A. Bioengineering Functional Copolymers XIV Synthesis and Interaction of Poly(*N*-Isopropyl Acrylamide-*co*-3,4-Dihydro-2H-Pyran-*Alt*-Maleic Anhydride) with SCLC Cancer Cells. *Bioorg. Med. Chem.* **2010,** *18,* 7975-7984.

[40] Türk, M.; Kahraman, G.; Khalilova, S. A.; Rzayev, Z. M. O.; Oguztüzün, S. Bioengineering Functional Copolymers. XVII. In teraction of Organoboron Amide-Ester Branched Derivatives of Poly(Acrylic Acid) with Cancer Cells. *J. Cancer Therapy* **2011,** *2,* 266-275.

[41] Rzayev, Z. M. O.; Türk, M.; Söylemez, E. A. Bioengineering Functional Copolymers XXI Synthesis of a Novel End Carboxyl-Trithiocarbonate Functionalized Poly(Maleic Anhydride) and Its Interaction with Cancer Cells. *Bioor. Med. Chem.* **2012,** *20,* 5053-5061.

[42] Lai, J. T.; Filla, D.; Shea, R. Functional Polymers from Novel Carboxyl-Terminated Trithiocarbonates as Highly Efficient RAFT Agents. *Macromolecules* **2002,** *35,* 6754-6756.

[43] Kedde, J.; Moad, G.; Rizzardo, E.; Thang, H. RAFT Agent Design and Synthesis. *Macromolecules* **2012,** *45,* 5321-5342.

[44] Rzayev, Z. M. O.; Söylemez, E. A. Functional Copolymer/Organo-MMT Nanoarchitectures VI Synthesis and Characterization of Novel Nanocomposites by Interlamellar Controlled/Living Radical Copolymerize-Tion via Preintercalated RAFT-Agent/Organoclay Complexes. *J. Nanosci. Nanotechnol.* **2011,** *11,* 3523-3532.

[45] Jenkins, R.; Snyder, R. L. *Introduction to X-ray Powder Diffractometry*; John Wiley & Sons Inc.: New-York, 1996; pp 89-91.

[46] Moreno-Fuquen, R.; Grande, C.; Advincula, R. C.; Tenorio, J. C.; Ellena, J. 2.2'-Carbonothioyldisulfanediyl)bis(2-Methylpropanoic Acid). *Acta Cryst. E* **2013,** *69,* 774-776.